Supplementary Figures

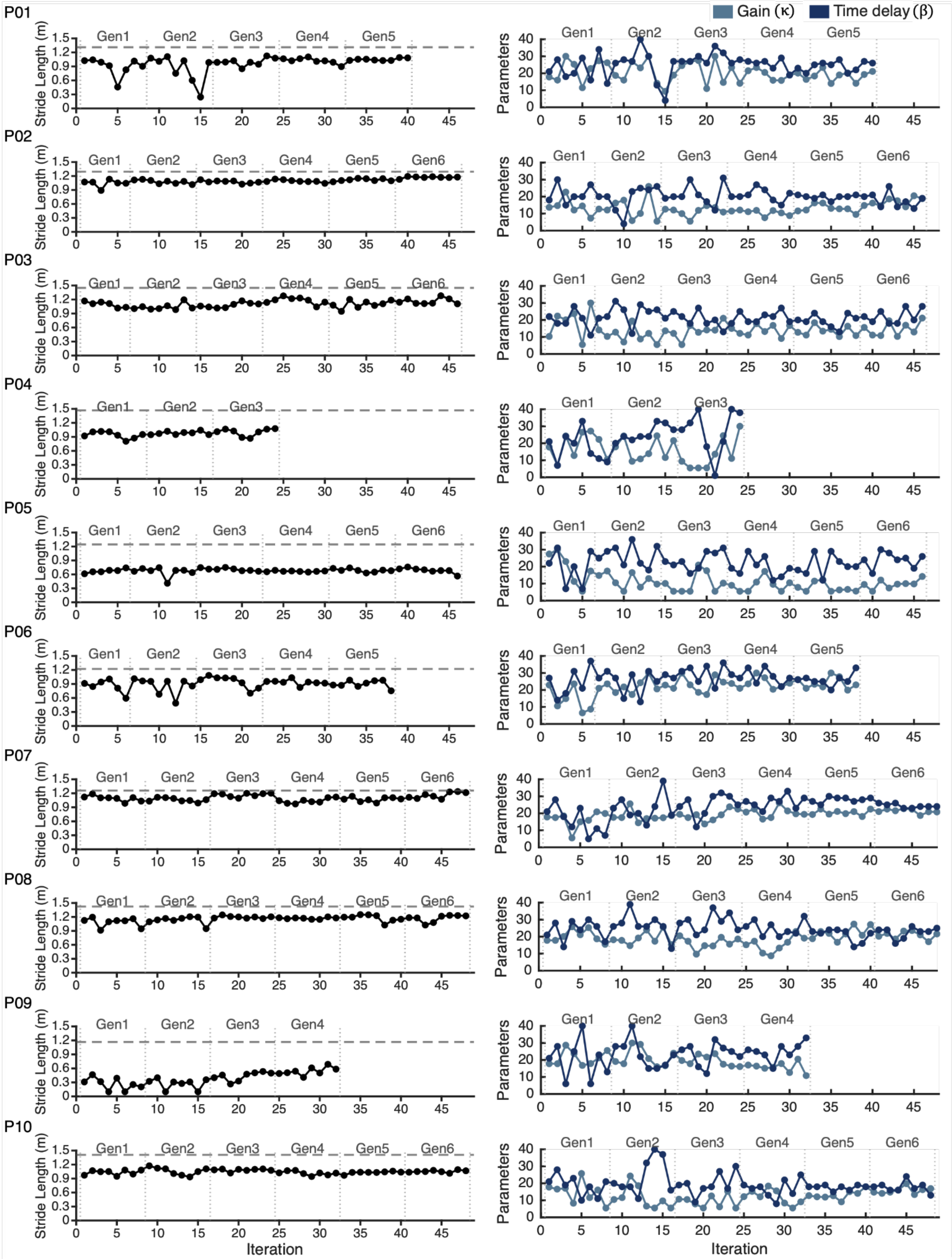

Supplementary Fig.1 Iterative optimization results across participants (P01-P10). The left panels show stride length evolution over iterations, with horizontal dashed lines indicating the average value reported in the literature for healthy individuals matched by age, sex, and height [1]. The right panels present corresponding parameter changes, including gain (light blue) and time delay (dark blue).

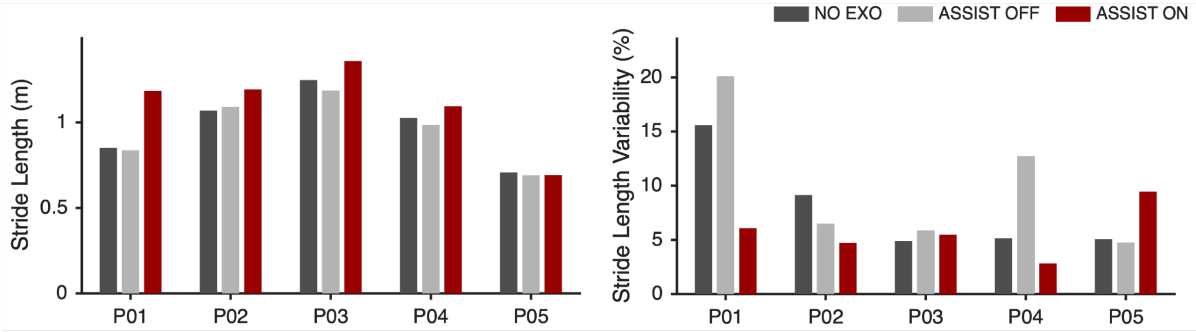

Supplementary Fig.2 Differences in changes under the ASSIST ON condition between P05 and P01–P04. Stride length (left) and stride length variability (right) for participants P01–P05 under three conditions.

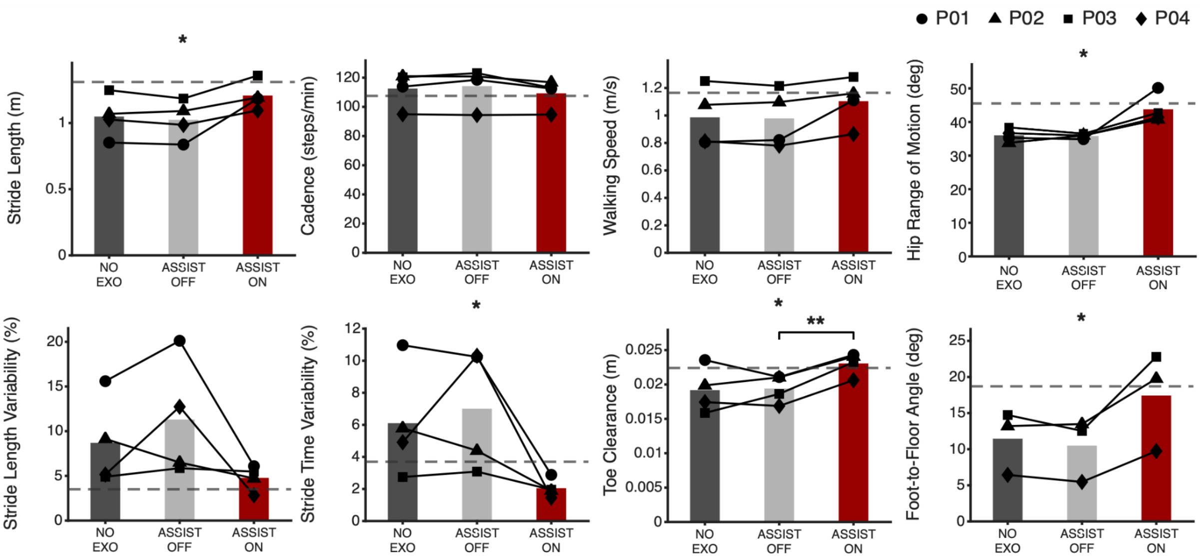

Supplementary Fig.3 Effects of personalized exoskeleton assistance on IMU-derived gait metrics during the Biomechanics Evaluation Day. Bars represent group means, while black lines with markers indicate individual participants. The horizontal dashed line denotes the mean value of a healthy control group reported in the literature [1–5]. Statistical significance is indicated as ** p < 0.01, * p < 0.05; only significant differences are indicated.

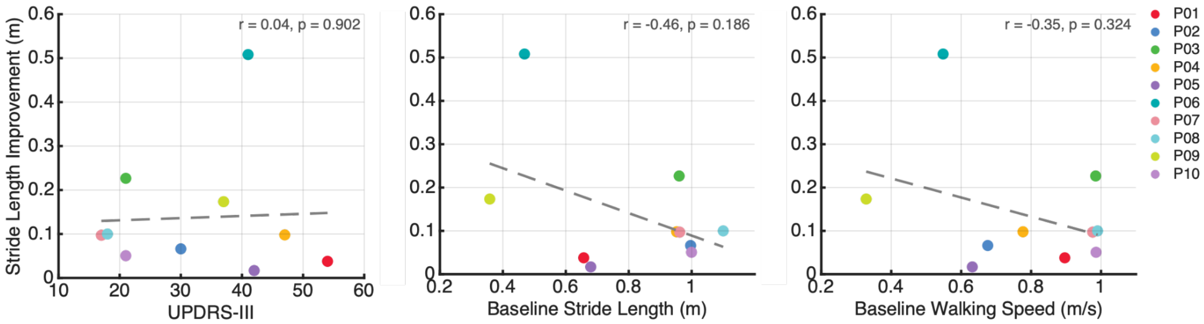

Supplementary Fig. 4 Relationship between baseline conditions and stride length improvement across participants. Linear regression coefficients (r) and p-values (p) are indicated in the top-right corner of each plot. Dashed lines represent the fitted linear regression lines. (A) Relationship between UPDRS part III scores and stride length improvement. (B) Relationship between baseline stride length under the ASSIST OFF condition and stride length improvement. (C) Relationship between baseline walking speed under the ASSIST OFF condition and stride length improvement.

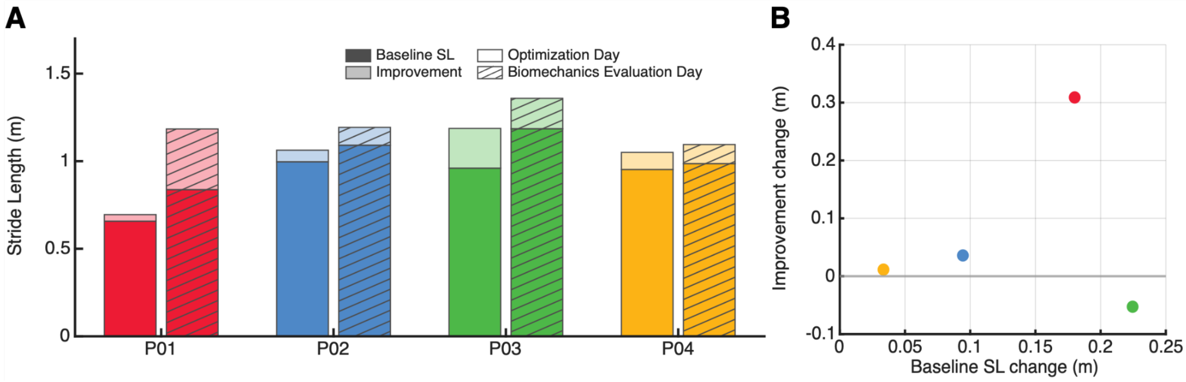

Supplementary Fig. 5 Differences in stride length improvement across days and participants. (A) Differences in stride length improvement across participants for each day. The dark portion of each bar represents baseline stride length (Baseline SL) under the ASSIST OFF condition, and the light portion represents the increase in stride length relative to baseline under the ASSIST ON condition. Non-hatched bars indicate results from the Optimization Day, whereas hatched bars indicate results from the Biomechanics Evaluation Day. (B) Changes in baseline stride length versus changes in stride length improvement.

Supplementary Table

Supplementary Table 1 Changes in gait metrics during the Optimization Day

ID	Stride Length (m)		Cadence (steps/min)		Walking Speed (m/s)		Hip Range of Motion (deg)		Foot-to-floor Angle (deg)		Stride Time Variability (%)	
	ASSIST OFF	ASSIST ON	ASSIST OFF	ASSIST OFF	ASSIST OFF	ASSIST OFF	ASSIST OFF	ASSIST ON	ASSIST OFF	ASSIST ON	ASSIST OFF	ASSIST ON
1	0.66	0.69	164	21.0	2.2	3.34	3.34	5.4	21.0	23.0	3.34	1.60
2	1.00	1.06	118	32.6	11.5	2.03	2.03	16.3	32.6	38.0	2.03	1.60
3	0.96	1.19	137	25.9	6.3	3.51	3.51	15.3	25.9	34.9	3.51	2.97
4	0.95	1.05	101	33.6	5.7	4.42	4.42	10.9	33.6	38.2	4.42	1.15
5	0.68	0.70	122	30.8	5.5	3.83	3.83	6.9	30.8	31.4	3.83	4.51
6	0.47	0.98	152	21.7	2.6	10.16	10.16	15.5	21.7	43.3	10.16	1.30
7	0.96	1.06	133	39.4	9.8	7.15	7.15	17.9	39.4	40.3	7.15	1.52
8	1.10	1.20	114	30.9	8.5	1.25	1.25	13.7	30.9	36.4	1.25	2.52
9	0.36	0.53	116	14.2	2.7	2.09	2.09	5.7	14.2	21.0	2.09	1.58
10	1.00	1.05	129	33.2	10.7	3.25	3.25	14.0	33.2	37.3	3.25	1.15

Supplementary Methods

Human-in-the-loop Optimization (HILO)

Determination of the number of iterations for convergence via Human-in-the-loop Optimization simulation

The human-in-the-loop optimization (HILO) experiments require a substantial amount of time, as sufficient walking data must be collected for each condition. Extensive pilot testing in participants with PD is limited by practical constraints, and selecting appropriate iteration numbers and convergence criteria is challenging in practice. Therefore, we first conducted simulations to determine an appropriate number of iterations and establish rational stopping criteria before conducting the clinical experiments. The overall simulation framework was implemented following the methodology described in the referenced study [6].

The parameter space consisted of two parameters: gain (κ) and time delay (β). Reasonable parameter bounds were determined through pilot testing in two healthy individuals instructed to mimic Parkinsonian gait under four walking conditions: (1) large step length with fast cadence, (2) small step length with fast cadence (shuffling gait), (3) large step length with slow cadence, and (4) small step length with slow cadence. Parameter combinations that were either excessively disruptive or provided insufficient gait assistance were excluded. Based on the pilot results, the final parameter bounds were set to 5.5–30 for gain (κ) and 0–40 for time delay (β).

Using these pilot-derived parameter bounds, simulations were then conducted to determine the number of iterations required for CMA-ES convergence. The objective function of the optimization algorithm in this study was defined as minimizing the difference between the target stride length, determined based on reference values from healthy individuals matched for age, sex, and height, and the participant's actual stride length measured during walking. The simulation modeled two key components affecting optimization performance: (1) the variation in the objective function over the parameter space and (2) measurement noise during objective function evaluation. The objective function was defined over a two-dimensional parameter space consisting of gain (κ) and time delay (β). The ground-truth objective function was assumed to have a single optimum, with the objective value increasing as the distance from the optimum increased over the normalized parameter space. Additive zero-mean Gaussian noise was introduced to emulate measurement uncertainty during stride length estimation. The noise level was determined from the error of IMU-based stride length estimates and motion capture-based stride length measurements. Specifically, the mean absolute error was computed under straight and counterclockwise walking conditions, and the resulting noise levels were combined using a weighted average (8:2) to reflect the experimental walking protocol.

The covariance matrix adaptation evolution strategy (CMA-ES) algorithm was originally developed for unconstrained optimization problems. To apply it to a constrained optimization setting, constraint-handling strategies are required when sampled points fall outside the feasible parameter space. In this study, we adopted the simple repair method, which projects infeasible samples onto the nearest feasible point, as it demonstrated the best performance among the tested methods in prior work [6].

The simulation indicated that the CMA-ES algorithm converged after approximately 78 evaluations, providing the rationale for the stopping criterion used in the experiments.

Convergence criteria were defined based on the change in the mean gain (κ) and mean time delay (β) parameters updated at each generation in the CMA-ES algorithm. Specifically, the optimization was considered converged when the mean parameter values of two consecutive generations satisfied $|\kappa^g - \kappa^{g-1}| < 1$ and $|\beta^g - \beta^{g-1}| < 5$ where κ^g and β^g denotes the mean gain and mean time delay parameters at generation g, respectively. These parameter resolutions were empirically determined through pilot testing in two healthy adults as the smallest changes in each parameter that produced a perceptible difference in the robotic assistance.

Covariance matrix adaptation evolutionary strategy (CMA-ES)

A Covariance Matrix Adaptation Evolution Strategy (CMA-ES) was employed to optimize two control parameters—gain (κ) and time delay (β) (Fig. 1A)—that determine the torque profile of the robotic device. The objective was to minimize the difference between each participant's actual and target stride lengths.

CMA-ES operates by adapting the search distribution to align with the contour of the objective function, thereby enabling efficient convergence toward the global optimum while reducing the number of function evaluations. An overview of the algorithm is provided below.

The algorithm begins by evaluating a set of candidate parameter samples constituting a single generation. These samples are drawn from a multivariate normal distribution defined by a mean vector, covariance matrix, and step size (standard deviation). The mean represents the current estimate of the optimal parameter values, while the population size (λ) is determined based on the number of parameters (n) to be optimized (e.g., $\lambda = 6$ for $n = 2$).

In this study, convergence was accelerated by modifying the sampling strategy. From the second generation onward, eight samples were evaluated by augmenting the original six samples with the mean of the previous generation and the best-performing sample from that generation. Based on simulation results of human-in-the-loop optimization, the number of iterations required for convergence decreased from 78 to 46. Accordingly, four participants (P02, P03, P05, and P06) completed 46 iterations. For the remaining participants (N = 6), two additional samples were evaluated. Specifically, the first generation consisted of eight samples, including both the mean of the initial distribution and the average of the optimal parameter values obtained from previously optimized participants. Consequently, the remaining participants (N = 6) completed 48 iterations.

After evaluating each generation, all parameter sets were ranked based on their performance. A rank-weighted average of the top-performing samples (e.g., the top three when $n = 2$) was then used as the mean for the subsequent generation. In addition, the covariance matrix was updated based on the distribution of high-performing samples. Multi-generational correlations were further incorporated to refine both the covariance matrix and the step size. Based on simulation results, the algorithm stopping criterion was defined as 48 iterations. The mean of the final generation was taken as the estimated optimal parameter set.

IMU-Based Gait Metrics

IMU-based gait metrics were obtained using a multi-stage processing pipeline consisting of walking bout identification, gait event detection, drift-corrected trajectory estimation, and outcome metric computation. The pipeline was implemented in Python and processed IMU data collected at a sampling frequency of 120 Hz.

Walking bout identification

For all experimental days, a control IMU, operated by a member of the study team, was deliberately shaken at the beginning and end of each trial to mark its temporal boundaries. During the Biomechanics Evaluation Day, additional shake events were introduced to delineate straight-walking segments. These events were detected using the magnitude of the control IMU acceleration, and adjacent shake events were used to partition each trial into alternating straight-walking and turning intervals. All detected segments were verified against synchronized video recordings to ensure accurate classification of steady-state (straight) and turning walking periods.

Gait event detection

Within each walking bout, heel-strike and toe-off events were identified from the angular velocity signals of foot-mounted IMUs [7]. The angular velocity profile exhibits characteristic features throughout the gait cycle, including a prominent peak representing the mid-swing phase. Mid-swing events were first detected using a threshold-based criterion on the sagittal-plane angular velocity, with a minimum temporal separation enforced between consecutive detections. The interval between successive mid-swing events was defined as a candidate stride cycle.

Within each stride cycle, local minima in the angular velocity profile were identified and grouped based on temporal proximity. The later cluster in the cycle was identified as the toe-off event, while the earlier cluster contained candidate heel-strike events. Heel-strike detection was further constrained to occur within a physiologically plausible temporal window relative to the adjacent toe-off events, and the most prominent candidate within this window was selected.

Drift-corrected trajectory estimation

To estimate foot trajectories, accelerometer signals of foot IMU were transformed into the global coordinate system using quaternions and integrated using a strapdown inertial navigation approach. Specifically, acceleration, $a(t)$, was first integrated to obtain velocity, $v(t) = \int a(t)\,dt$, which was subsequently integrated to estimate position, $p(t) = \int v(t)\,dt$.

To mitigate drift caused by double integration of noisy IMU signals, a combined Zero-velocity Update (ZUPT) and linear drift correction method was applied [8]. During the mid-stance phase, when the foot was assumed to be stationary, the velocity was reset to zero, $v(t_i) = 0,\ t_i \in T\_\text{mid-stance}$.

To compensate for drift between consecutive zero-velocity intervals, a linear drift model was assumed. Let $v(t_{j+1})$ denote the residual velocity at the end of an interval. The drift was approximated as linearly accumulating over time and removed as $v_{cor}(t) = v(t) - ((t - t_j) / (t_{j+1} - t_j)) * v(t_{j+1}),\ t \in [t_j , t_{j+1}]$. The corrected velocity was then integrated to reconstruct the drift-compensated three-dimensional foot trajectory.

Computation of outcome metrics

Using the detected gait events and reconstructed trajectories, spatiotemporal gait parameters were computed for each walking bout. During the Optimization Day, a 40-s walking trial was analyzed after excluding the initial 15 s and the final 5 s to remove transient effects. During the Biomechanics Evaluation Day, data from the 2-minute walk test (2MWT) were analyzed after excluding the first and last 5 s. Stride length was defined as the Euclidean distance L_k between the three-dimensional foot positions $p(t_k)$ at consecutive heel-strikes of the same foot, $L_k = \|p(t_{k+1}^{HS}) - p(t_k^{HS})\|$. Cadence was calculated as the number of steps (N_{steps}) per minute across both feet, cadence = $(N_{steps} / T_{bout})*60$, where T_{bout} denotes the total bout time. Walking speed v_k was computed on a per-stride basis as $v_k = L_k / T_k$ and averaged across each trial. Gait variability was quantified using the coefficient of variation (CV), $CV = (\sigma / \mu) \times 100\%$, where μ and σ denote the mean and standard deviation of a given parameter across strides. Toe clearance was calculated from the vertical toe trajectory as the difference between the local minimum near toe-off and the subsequent local minimum during swing. To estimate the vertical toe trajectory, the approximate toe position was reconstructed by applying a fixed offset to the position and orientation of the IMUs attached to the lateral malleolus.

Foot-to-floor angle was derived from the time-series of the angle between the foot forward direction vector and the horizontal plane, computed from the IMU-derived orientation. For each heel-strike event detected from the IMU angular velocity signal, a 0.25 s temporal window centered on the event was defined, and the peak angle value within this window was identified. The foot-to-floor angle was defined as the difference between this peak value and the subsequent foot-flat angle. The foot-flat angle was determined as the median value within a window corresponding to 10–30% of the gait cycle following the identified peak. This interval range was selected based on visual inspection of the angle profile.

Hip motion was estimated from thigh-mounted IMU signals, with the resulting thigh angular excursions used as a proxy for hip range of motion. For each limb, hip range of motion was computed on a per–gait cycle basis as the difference between the maximum flexion and maximum extension angles within each cycle, and then averaged across all cycles within a walking bout, Hip range of motion = $(1 / N) * \sum_{k=1}^{N} [\max_{t \in C_k} \theta(t) - \min_{t \in C_k} \theta(t)]$, where $\theta(t)$ is the thigh angle, C_k is the k-th gait cycle, and N is the total number of cycles.

Motion Capture Analysis

Video data of Biomechanics Evaluation Day were recorded at sampling frequency of 100Hz, processed using Theia3D, and further analyzed using Visual3D (C-Motion Inc., Germantown, MD, USA) and MATLAB (MathWorks Inc., Natick, MA, USA). Data processed through Theia3D provide three-dimensional anatomical landmark positions, as well as body segment positions and orientations.

Time-series data of joint angles and angular velocities, additional time-series data required to derive joint-based metrics (i.e., foot, trailing limb, and trunk angles), and gait events were obtained through further processing in Visual3D. All joint angles, angular velocities, and derived angles were analyzed in the sagittal plane. Hip, knee, and ankle joint angles and angular velocities were defined as the relative angles between adjacent body segments. For the computation of average trunk flexion, the angle between the trunk segment and the vertical axis was projected onto the sagittal plane to obtain the trunk flexion angle. Similarly, for the computation of foot-to-floor angle, the foot angle was defined as the angle between the foot segment and the anterior-posterior axis projected onto the sagittal plane. The trailing limb angle was defined as the angle between the line connecting the hip and toe landmarks and the vertical axis, projected onto the sagittal plane. For gait event detection, heel strikes were identified using a method similar to that of Hreljac and Marshall [9] by detecting local maxima in the vertical acceleration of the heel landmark.

Using time-series data of anatomical landmark positions, joint angles, angular velocities, and derived angles, gait outcome metrics were computed in MATLAB. All time-series data were filtered using a fourth-order Butterworth low-pass filter with a cutoff frequency of 6 Hz. Biomechanical analyses were restricted to the straight walking region. Only gait cycles in which the mid-hip landmark position remained within the predefined region were included.

Joint angle and angular velocity profiles of the hip, knee, and ankle were averaged across strides and sides for each participant. Gait cycles were segmented based on heel-strike events detected as described earlier. Each segmented cycle was time-normalized to 201 data points, with 0% of the gait cycle corresponding to heel strike. Range of motion was defined as the difference between the maximum and minimum values within each stride. Peak velocities were extracted within each stride at predefined phases of the gait cycle. Strides in which peak detection was unsuccessful were excluded from the analysis.

For each stride, the walking direction was defined as the displacement vector of the heel marker between consecutive heel-strikes of the same foot in the horizontal plane. Step length was calculated as the component of the vector from the heel position at heel-strike to the contralateral heel position at the subsequent heel-strike, projected onto the walking direction. Step width was defined as the component of this vector perpendicular to the walking direction. Toe clearance was calculated from the vertical toe marker trajectory as the difference between the local minimum near toe-off and the subsequent local minimum during swing. Foot-to-floor angle was defined as the peak foot angle occurring immediately after heel-strike. Maximum trailing limb angle was defined as the peak extension of the trailing limb angle within each stride. Average trunk flexion was computed as the mean trunk angle over each stride.

For each walking condition, average trunk flexion was computed from gait cycles segmented using right heel-strike events only. For all other metrics, values were first averaged across strides separately for each side (left/right), and the mean of these two values was then taken. For participants who performed repeated trials under the same condition, gait metrics were further averaged across trials within each condition.

References

1. Samson MM, Crowe A, De Vreede PL, Dessens JAG, Duursma SA, Verhaar HJJ. Differences in gait parameters at a preferred walking speed in healthy subjects due to age, height and body weight. Aging Clin Exp Res. 2001;13:16–21. https://doi.org/10.1007/BF03351489

2. Vette AH, Watt JM, Lewicke J, Watkins B, Burkholder LM, Andersen J, et al. The utility of normative foot floor angle data in assessing toe-walking. The Foot. 2018;37:65–70. https://doi.org/10.1016/j.foot.2018.07.003

3. Hollman JH, McDade EM, Petersen RC. Normative spatiotemporal gait parameters in older adults. Gait Posture. 2011;34:111–8. https://doi.org/10.1016/j.gaitpost.2011.03.024

4. Bohannon RW, Wang Y-C, Gershon RC. Two-Minute Walk Test Performance by Adults 18 to 85 Years: Normative Values, Reliability, and Responsiveness. Arch Phys Med Rehabil. 2015;96:472–7. https://doi.org/10.1016/j.apmr.2014.10.006

5. Begg R, Best R, Dell'Oro L, Taylor S. Minimum foot clearance during walking: Strategies for the minimisation of trip-related falls. Gait Posture. 2007;25:191–8. https://doi.org/10.1016/j.gaitpost.2006.03.008

6. Collins SH, Wiggin MB, Sawicki GS. Reducing the energy cost of human walking using an unpowered exoskeleton. Nature. 2015;522:212–5. https://doi.org/10.1038/nature14288

7. Jasiewicz JM, Allum JHJ, Middleton JW, Barriskill A, Condie P, Purcell B, et al. Gait event detection using linear accelerometers or angular velocity transducers in able-bodied and spinal-cord injured individuals. Gait Posture. 2006;24:502–9. https://doi.org/10.1016/j.gaitpost.2005.12.017

8. Suresh RP, Sridhar V, Pramod J, Talasila V. Zero Velocity Potential Update (ZUPT) as a Correction Technique. 2018 3rd Int Conf Internet Things Smart Innov Usages IoT-SIU [Internet]. Bhimtal: IEEE; 2018 [cited 2026 Apr 30]. p. 1–8. https://doi.org/10.1109/IoT-SIU.2018.8519902

9. Hreljac A, Marshall RN. Algorithms to determine event timing during normal walking using kinematic data. J Biomech. 2000;33:783–6. https://doi.org/10.1016/S0021-9290(00)00014-2